Bull. Chem. Soc. Jpn., 71, 99—112 (1998)

Theoretical Studies of Multiple Metal–Metal Bonds between Divalent Molybdenum Ions in Dimers, Tetramers, and Clusters

Masamichi Nishino, Yasunori Yoshioka, Kizashi Yamaguchi,* Kazushi Mashima,*,†

Kazuhide Tani,† and Akira Nakamura††

Department of Chemistry, Graduate School of Science, Osaka University, Toyonaka, Osaka 560

†Department of Chemistry, Graduate School of Engineering Science, Osaka University, Toyonaka, Osaka 560

††Department of Macromolecular Science, Graduate School of Science, Osaka University, Toyonaka, Osaka 560

(Received August 4, 1997)

The multiple metal–metal bonds between divalent molybdenum (Mo(II)) ions in dimers and tetramers were investigated theoretically. The orbital energy gaps, occupation numbers of natural orbitals (NO) and effective bond orders for the naked $Mo(II)_2$ dimer (**1**) were calculated by ab initio UHF MO and density functional (DFT) methods. The effective exchange integrals (J_{ab}) of **1** were calculated by approximately spin-projected UHF and DFT methods, and the complete active space (CAS) CI by the use of UHF NO. The calculated J_{ab} values were discussed in relation to the temperature-dependent paramagnetism observed for the edge-sharing and face-sharing bioctahedral molybdenum complexes. The CAS CI calculations showed that the Heisenberg model is not appropriate for **1** under the condition that the Mo–Mo distance is shorter than 2.5 Å. The UHF and DFT MO calculations were also performed for the linear naked $Mo(II)_4$ tetramer (**2**) to elucidate possible electronic structures of the d–d conjugated systems. The continuous changes from closed-shell (diamagnetic) electronic structures to antiferromagnetic states were investigated by elongating the Mo–Mo distances. Similarities and differences between $Mo(II)_2$ (**1**) and naked $Cr(II)_2$ (**3**) or between $Mo(II)_4$ (**2**) and $Cr(II)_4$ (**4**) were examined and compared, since the nature of direct exchange couplings between divalent chromium ions in **3** and **4** was already studied extensively in relation to the electron correlation effect. The metal-insulator transitions induced by elongation of the Mo(II)–Mo(II) distance in Mo(II) clusters were discussed from the viewpoint of electron correlation and size effects in mesoscopic systems.

The multiple metal–metal bonds between transition metals have been investigated extensively by Cotton and his collaborators.[1—3] It is well-established that the dimolybdenum compounds, $Mo_2(II)X_8L_2$, possess $\sigma^2\pi^4\delta^2$ electronic configurations, and therefore involve the cores of dinuclear divalent molybdenum ions $Mo(II)_2$ (**1**) with quadruple metal–metal bonds. The Mo(II)–Mo(II) distances are determined to be in the order: 2.04—2.21 Å, so the atoms exhibit the diamagnetism.[2] Theoretically polymerizations of this quadruple bond are conceivable to afford conjugated metal polymers like polyacetylene as organic analogs. The linear tetranuclear clusters with $Mo(II)_4$ (**2**) cores would be interesting synthetic targets in this category, but there are no reports about such polymer complexes, though other linear transition metal complexes such as Pt_8 and Pt–Mo_2–Pt complexes have been synthesized, respectively, by Matsumoto et al.[4] and Mashima et al.[5,6] On the other hand, edge-sharing bioctahedral compounds of trivalent molybdenum with the d^3–d^3 interactions have usually stable $\sigma^2\pi^2\delta^2$ or $\sigma^2\pi^2(\delta^*)^2$ configurations with the diamagnetism. However, the observed effective exchange integrals (J_{ab}) for several dimolybdenum compounds such as Mo_2Cl_6 $(dppe)_2$[7—9] are in the range; −340——470 cm^{-1}. Therefore these compounds exhibit the temperature-dependent paramagnetism. The face-sharing bioctahedral compounds of trivalent molybdenum, $[Mo(III)_2X_9]^{3-}$, showed that the Mo(III)–Mo(III) distances varied over the range 2.5—2.8 Å, depending on the crystalline environments.[10—12] These compounds exhibited a good correlation between the Mo–Mo distances and the paramagnetic susceptibilities.[7—12]

The nature of multiple bonds between transition metal ions in binuclear complexes has been studied theoretically.[13—22] For example, strong quadruple bonds between Mo(II) ions in various $Mo(II)_2X_8$ complexes have been investigated by the spin-restricted SCF-Xα-SW method.[18,22] Their σ, π, and δ-bonding schemes[1—3] and orbital configurations $(\sigma)^2(\pi)^4(\delta)^2$ are now well understood on the basis of the closed-shell molecular orbital picture. The ionization potentials and orbital energy levels revealed by the photoelectron spectroscopy[23] are wholly consistent with these theoretical results.[16—22] On the other hand, the quadruple bonds between Cr(II) ions in $Cr(II)_2(O_2CR)_4L_2$ complexes (R = H, CH_3, L = H_2O, etc.) are rather weak because of strong electron-correlation effects,[13—15] leading to its valence-bond (VB) type description.[24—26] In fact, the large variability of the Cr–Cr distances, a range of 0.3 Å, depending on axial ligands has been experimentally elucidated,[2] and this may indicate that the potential energy curve for the $Cr(II)_2$ unit

is rather shallow, in conformity with the instability of the Cr–Cr bond.[17,27] The Cr–Cr bond distances in the complexes have been calculated by several electron-correlated techniques such as APSG,[16] RHF-CI,[17] limited MC-SCF[19] and GVB[20] methods, together with Hartree–Fock–Slater (HFS) transition state method.[21] However, the calculated distances were too long even at the perfect-pairing (PP) GVB level,[20] which involved the pair correlation for the quaduple bond. Thus multiple bonds between Cr(II) ions raise exceptional challenges to the theory of unstable metal–metal (M–M) bonds.[24–26] Since the M–M quadruple bonds include key elements in most other multiple bonds, theoretical study of them is indeed essential.

Although the extended Hückel calculations[28] have been already carried out for the d–d conjugated systems, they do not account for electron–electron interactions, which play crucial roles in magnetism.[2,13,27] In fact, a model calculation[13] showed that the electron correlation effect is remarkable for the Cr–Cr bond. Ab initio Hartree–Fock and density functional (DFT) studies on these clusters are therefore desirable in this regard. In a previous paper,[29], we have examined several theoretical approaches to direct exchange couplings between divalent chromium ions in naked dimers (**3**), tetramers (**4**), and clusters. It was found that the orbital energy gaps are rather small for **3** and therefore the occupation numbers of the bonding σ-, π-, and δ-molecular orbitals and formal quadruple bond orders were largely reduced because of strong electron correlation effects. The reliability of the Heisenberg-model Hamiltonian was elucidated from variations of these calculated effective exchange integrals with the interatomic distance. The calculated J_{ab} values[14] were compared with the experimental results[10–12] for several binuclear Cr(II) complexes with different interatomic distances.

The metal–metal bonds between second- and third row transition metals are usually stable, exhibiting no magnetism. The closed-shell pictures by spin-restricted Xα SW method are reliable for the species.[22] However, there are several unusual cases even for molybdenum complexes mentioned above. As a continuation of previous work,[29] we here examine several theoretical approaches to the d–d conjugated systems of **1** and **2**. First, the quadruple metal–metal bonds of **1** are investigated by ab initio UHF and DFT methods, and complete active space (CAS) configuration interation (CI) methods based on the UHF natural orbital (UNO).[29] The occupation numbers of the occupied σ-, π-, and δ-orbitals and formal quadruple bond orders are calculated by these methods. The energy differences among singlet, triplet and quintet states for **1** are also calculated from the total energies obtained by the UNO CASCI method to elucidate differences between the metal–metal bonds of Mo(II) and Cr(II). The UHF and DFT MO calculations are also performed for **2** to elucidate possible electronic structures of the d–d conjugated systems. The difference of electron correlation effects between linear naked $Mo(II)_4$ and $Cr(II)_4$ tetramers is investigated theoretically. The metal–insulator transitions induced by elongation of the Mo(II)–Mo(II) distance are explained by localizations of different-orbitals-for-different-spins (DODS) MOs for **2**.[27] Implications of the calculated results were discussed in relation to the temperature-dependent paramagnetism for edge- and face-sharing molybdenum complexes,[7–12] and in relation to quantum spin tunneling for magnetic clusters.[29]

Generalized Molecular Orbital Description of Binuclear Quadruple Bonded Systems

1. Ab Initio MO Calculations. Cotton et al.[1–3] have extensively investigated the quadruple metal (M)–metal (M) bonds for the M_2X_8 complexes (M = Cr, Mo, Re, etc.). The transition metal ions MX_4 in these dimers are formally regarded as the d^4 configuration with the octahedral (Oh) ligand field. The divalent molybdenum dimer $Mo(II)_2$(**1**) is also regarded as a d^4–d^4 system with a quadruple bond.[13–22] Quadruple M–M bonds have been described as the $\sigma^2\pi^4\delta^2$ orbital configuration on the basis of the spin-restricted MO-theoretical picture. However, the strong electron correlation effect may reduce the formal bond order as in the cases of the direct exchange-coupled manganese dimer (**5**)[30a] and chromium dimer (**6**)[30b] and superexchange coupled transition-metal complexes (**7**)[30c,30d] examined previously (Scheme 1).

The ab-initio UHF MO calculations of **1** are carried out using a Tatewaki–Huzinaga basis set[31] [4333/433/4] which is supplemented by the 4p-AO with the same exponent as that for the 4s-AO. The basis set dependency of the bonding characteristics was examined previously,[29] showing that this single zeta (SZ) basis set is qualitatively useful to elucidate the electronic structures of species containing the transition metals. The SZ basis set is, thefore, also utilized for the spin-unrestricted (U) DFT calculations by the use of the Becke–Lee–Yang–Parr (U-BLYP) functional[32,33] and Becke's mixing (U-B2LYP) methods. In the latter approach, the original mixing ratio between the UHF and DFT exchange terms ($c_0 = 0.332$ and $c_1 = 0.575$) by Becke[32b] was taken throughout this work. The mixing of the DFT and UHF exchange potentials expects that the self-interaction correction for the DFT approach can be accomplished by this conventional hybrid technique. Though the optimization of the hybrid methods such as B3LYP and B10LYP are, there-

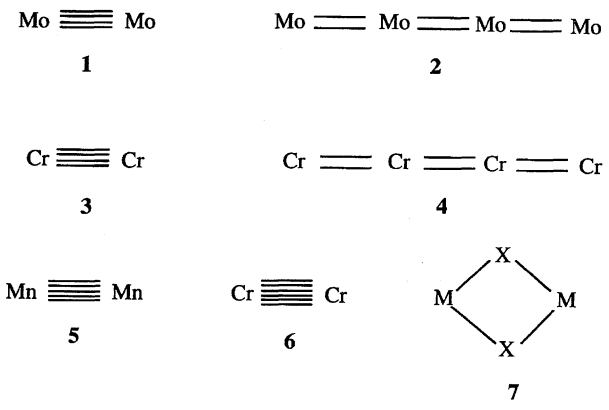

Scheme 1.

fore, out of our present concern, effective exchange integrals estimated by B3LYP will be shown as an example for comparison with B2LYP. All the MO computations were carried out on an IBM RS 6000 computer using the GAUSSIAN 94 program package.[34]

2. MO-Description of the Quadruple Bond.

The high-spin (HS) UHF and DFT solutions for **1** are easily obtained by spatial symmetry. The bonding and antibonding orbitals for the HS state of **1** are given by the symmetry-adapted MOs

$$\phi(\mathrm{X}) = N[\mathrm{dX_a} + \mathrm{dX_b}],\quad \phi^*(\mathrm{X}) = N'[\mathrm{dX_a} - \mathrm{dX_b}] \qquad (1)$$

where N (N') is the normalizing factor and dX denotes the d-atomic orbital symmetry, i.e., σ,π_x,π_y,δ_{xy}, and $\delta_{x^2-y^2}$. The σ, π, and δ-MOs by HS UHF solutions are symmetry-adapted like those of the extended Hückel MO and spin-restricted DFT scattered-wave (SW) methods.[18,22] The energy gap between the bonding and antibonding orbitals is sensitive to the d–d orbital interaction, as illustrated in Fig. 1. The orbital energy gaps are, therefore, calculated to elucidate the strength of the d–d orbital interactions by

$$\Delta\varepsilon_{\mathrm{Y}}(\mathrm{X}) = \varepsilon^*(\mathrm{X}) - \varepsilon(\mathrm{X}) \qquad (2)$$

where ε and ε^* denote, respectively, the orbital energies for bonding and antibonding MOs by the HS UHF (=Y) and DFT solutions.

Table 1 summarizes the calculated energy gaps for σ-, π-, and δ-MOs for **1** by UHF, together with U-BLYP and U-B2LYP. From Table 1, the energy gaps given for σ- and π-MOs by these methods are over 5 eV near the equilibrium distance (R=2.0 Å), showing the large energy gaps,

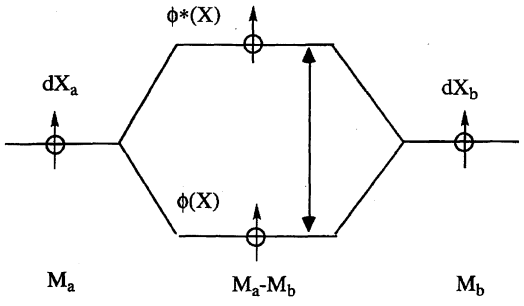

Fig. 1. The orbital interaction scheme for the d–d bond for transition metal dimer. The notations are given in the text.

though the value are a little different among the computational methods and decrease in the order for the σ–σ^* and π–π^* gaps: $\Delta\varepsilon(\mathrm{X})_{\mathrm{UHF}} > \Delta\varepsilon(\mathrm{X})_{\mathrm{U\text{-}B2LYP}} > \Delta\varepsilon(\mathrm{X})_{\mathrm{U\text{-}BLYP}}$. The orbital energy gaps for the δ–δ^* bond are smaller than 2.0 eV even near 2.0 Å. This small gap may entail the triplet instability for the closed-shell pair given by $|\phi(\mathrm{X})\overline{\phi}(\mathrm{X})|$ as shown in the case of naked Cr(II) dimer (**3**).[29] The bonding and antibonding δ-orbitals are nearly degenerate in energy at a relatively large interatomic distance (R>2.0 Å). This implies that δ-bond should suffer the triplet instability even near the equilibrium distance.[19]

The orbital energy gap becomes smaller than 4.0 eV even for the σ- and π-MOs when R exceeds 2.5 Å. In this situation, the closed-shell Hartree–Fock solution involves the so-called triplet instability. Because of the triplet instability, the bonding σ- and π-UHF MOs for the lowest spin LS (S=0) state of **1** are given by the left-right split-orbitals, which are described by mixing of the bonding and antibonding MOs in Eq. 1 as follows

$$\Psi^+(\mathrm{X}) = \cos\theta\phi(\mathrm{X}) + \sin\theta\phi^*(\mathrm{X}) = \cos\omega a(\mathrm{X}) + \sin\omega b(\mathrm{X}), \qquad (3a)$$

$$\Psi^-(\mathrm{X}) = \cos\theta\phi(\mathrm{X}) - \sin\theta\phi^*(\mathrm{X}) = \cos\omega b(\mathrm{X}) + \sin\omega a(\mathrm{X}), \qquad (3b)$$

where θ and ω are the MO- and VB-orbital mixing parameters, and a(X) and b(X) are the localized natural orbitals (LNO) defined by θ=45° as follows:[27]

$$a(\mathrm{X}) = 1/2\{\phi(\mathrm{X}) + \phi^*(\mathrm{X})\} = \mathrm{dX_a} \qquad (4a)$$

$$b(\mathrm{X}) = 1/2\{\phi(\mathrm{X}) - \phi^*(\mathrm{X})\} = \mathrm{dX_b} \qquad (4b)$$

The LNOs mainly localized on one site have generally small tails on the other site, satisfying the orthogonality condition, and they reduce to the corresponding atomic orbitals (AOs) at the dissociation limit. The different-orbitals-for-different-spins (DODS) MOs (Eq. 3) for the up- and down-spins in the singlet state of **1** are more or less localized on the left and right molybdenum atoms, respectively, because of electron correlations. The DODS MOs are also obtained by the U-BLYP and U-B2LYP[32b] calculations, although θ and ω in Eq. 3 are different among the three computational procedures employed here. As shown previously,[27] the DODS MOs are reduced to the symmetry-adapted MOs given by Eq. 1 at the weak correlation limit (MO limit; θ=0°), whereas they become equivalent to the LNO by Eq. 4 at the VB-limit (θ=45°).

As an example, let us consider variations of the dπ–dπ

Table 1. The Orbital Energy Gaps (eV) Calculated for the High-Spin State of the Naked Mo(II) Dimer (Mo_2^{4+}) by UHF, U-BLYP, and U-B2LYP Methods

R	$\Delta\varepsilon_{\mathrm{UHF}}$			$\Delta\varepsilon_{\mathrm{U\text{-}BLYP}}$			$\Delta\varepsilon_{\mathrm{U\text{-}B2LYP}}$		
Å	$\sigma\sigma^*$	$\pi\pi^*$	$\delta\delta^*$	$\sigma\sigma^*$	$\pi\pi^*$	$\delta\delta^*$	$\sigma\sigma^*$	$\pi\pi^*$	$\delta\delta^*$
2.000	7.705	6.634	1.641	6.592	5.550	1.398	6.770	6.420	1.682
2.0981	7.054	5.654	1.316	5.859	4.750	1.152	6.205	5.501	1.357
2.1208	6.912	5.447	1.250	5.732	4.576	1.093	6.085	5.306	1.291
2.500	3.943	2.854	0.527	3.861	2.309	0.459	4.327	2.839	0.558
3.000	2.618	1.134	0.167	2.005	0.896	0.149	2.467	1.177	0.183
3.500	1.176	0.424	0.055	0.903	0.346	0.051	1.205	0.467	0.061

bond with interatomic distance (R) between Mo(II) atoms. Figure 2 illustrates the π-type DODS MOs obtained for **1** at R=2.0, 2.5, and 3.0 Å by the U-B2LYP method. The π-orbitals for (A) at R=2.0 Å are symmetry-adapted, being equivalent to the closed-shell MOs (**8**) given by the spin restricted DFT calculations.[18,22] This is evidently different from the case of $Cr(II)_2$ (**3**).[29] On the other hand, they are almost localized on each atomic site at R=3.0 Å, describing the antiferromagnetic spin-coupling of **1**. The DODS π-orbitals at R=2.5 Å are more or less localized on the left- and right-MO(II) atoms, respectively, showing an intermediate characteristic, ·Mo(II)≡Mo(II)·(**9**), between two extremes (Scheme 2). In this intermediate electronic state, the energy difference between the ground and excited higher spin states becomes small with increasing thermal populations of the higher spin states at finite temperature. This situation causes the temperature-dependent paramagnetism. Figure 3 shows variations of the δ-orbitals of **1** at R=2.0 and 2.5 Å, respectively. The δ-DODS MOs for **1** are found to be spin-polarized and more or less localized on an atomic site even at R=2.0 Å, in conformity with the small δ–δ^* orbital energy gap in Table 1.

3. Occupation Numbers and Bond orders for Dinuclear Metal–Metal Systems. The preceding results clearly indicate that the MO and valence bond (VB) pictures are, respectively, useful for qualitative understanding of the bonding property of **1** at shorter and longer interatomic distances.

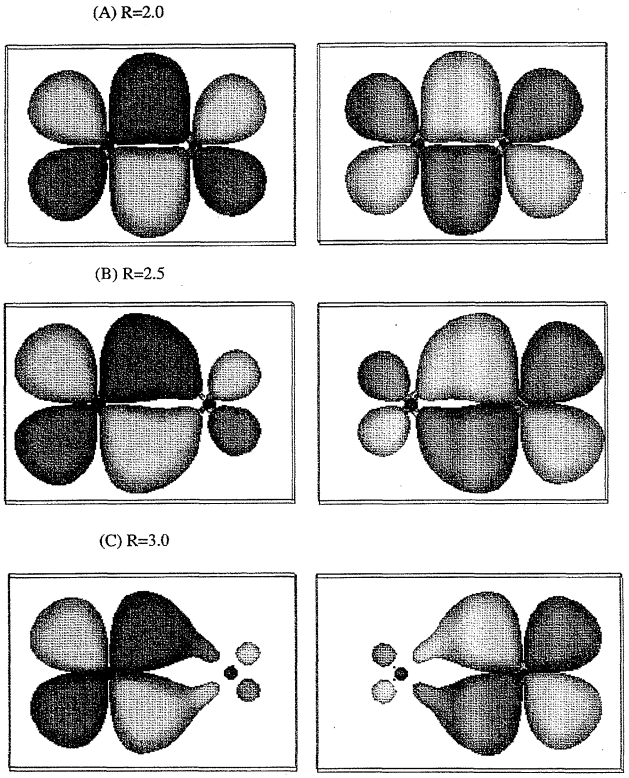

Fig. 2. The computer-graphics of the bonding π-type DODS MOs for the Mo(II) dimer (**1**) obtained by the U-B2LYP method. A, B, and C denote up (α) and down (β) spin orbitals at different interatomic distances (see text).

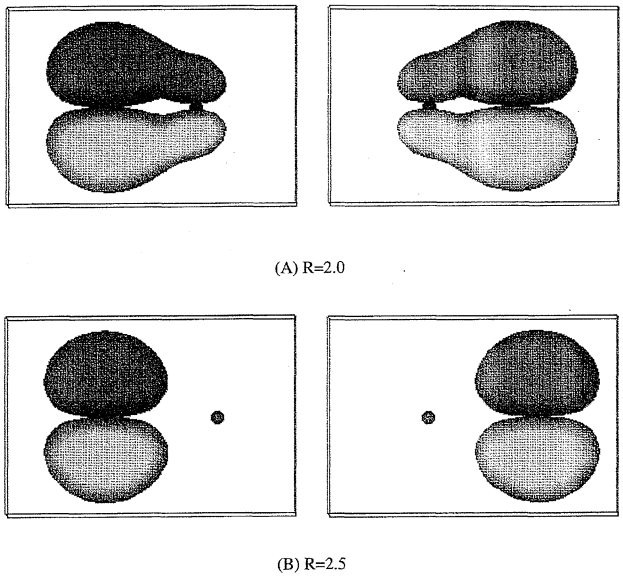

Fig. 3. The computer-graphics of the bonding δ-type DODS MOs for the Mo(II) dimer (**1**) obtained by the U-B2LYP method. A and B denote up (α) and down (β) spin orbitals at differece interatomic distances (see text).

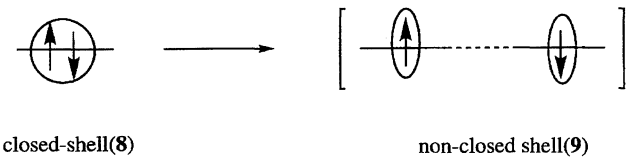

closed-shell(**8**) non-closed shell(**9**)

Scheme 2.

On the other hand, it is noteworthy that the UHF and DFT molecular orbitals for the up- and down-spins are largely localized on the left and right Cr(II) ions even at a short distance for **3**.[29] To elucidate this difference quantitatively, the occupation numbers in the perfect-pairing-type spin-projected UHF or U-BLYP solutions and their effective bond orders are calculated.[35,36]

Figure 4 shows variations of the occupation numbers with R obtained for the σ-, π-, and δ-MOs (Eq. 4) by the spin-projected UHF and U-BLYP solutions. Table 2 summarizes the effective bond orders calculated for **1**. From Table 2, and Figure 4, the following results are available.

(1) The occupation number of each bonding orbital for the d^4–d^4 exchange-coupled system **1** by UHF decreases sharply with the increase of interatomic distance (R).

(2) On the other hand, the occupation numbers of σ- and π-NOs by DFT are almost 2.0 in the region; 2.0 Å$<R<$2.5 Å. Functional behaviors with R concluded from projected (P) U-BLYP and PU-B2LYP are quite different from that of PUHF.

(3) The occupation numbers calculated for the σ- and π-NOs indicate the following tendency: n_X(PU−BLYP)$>$ n_X(PU−B2LYP)$>n_X$(PUHF) ($X=\sigma$ or π). Probably, the PUHF provides the lower limit for the bond order, whereas the PU-BLYP gives the upper limit.

(4) The occupation numbers of each bonding orbital for **1** by PU-B2LYP are smaller than the formal value, 2.0 in the re-

Table 2. The Effective Bond Orders for the Mo(II) Dimer (**1**) by the PP-Type Projected UHF, U-BLYP, and U-B2LYP Methods

R	PUHF			PU-B2LYP			PU-BLYP		
Å	σ	π	δ	σ	π	δ	σ	π	δ
2.0000	0.955	0.940	0.371	1.000	1.000	0.754	1.000	1.000	0.969
2.0981	0.922	0.880	0.294	1.000	0.999	0.620	1.000	1.000	0.885
2.1208	0.914	0.863	0.278	0.999	0.999	0.589	1.000	1.000	0.860
2.5000	0.740	0.545	0.115	0.970	0.864	0.235	0.998	0.977	0.379
3.0000	0.461	0.236	0.037	0.772	0.453	0.076	0.929	0.643	0.118
3.5000	0.233	0.094	0.012	0.455	0.192	0.025	0.641	0.299	0.041

gion: $R<2.5$ Å. Therefore, the coresponding bond order for each bond is also smaller than 1.0. Judging from the occupation number and bond order, one concludes that the δ–δ bond is particularly weak, in accord with the experiments.[1—3] (5) The bond orders of the π and σ bonds for **1** are larger than 0.8 if $R<2.5$ Å, and therefore the Mo(II)–Mo(II) bonds in the core are rather stable, compared with those of the Cr(II)–Cr(II) system.[29]

From these conclusions, the perfect-pairing (PP)-type projection[29] is useful for qualitative descriptions of the d–d bonding properties for the LS state. The dramatic change of the nature of Mo–Mo bond indicates the sharp decrease of the σ- and π-bond orders in the region; $2.4<R<2.8$ Å, suggesting (a) that the magnitude of effective exchange integrals should change sharply in this region, (b) that the nonlinear response properties for external electromagnetic fields (second hyperpolarizability, hypermagnetiability, etc.) exhibit characteristic variations because of electron fluctuation,[37,38] and developments of appropriate ligands to control Mo–Mo distances are necessary for optimizations of electronic properties under consideration.

4. Effective Exchange Integrals. When the energy difference between the ground and excited higher spin states becomes small, thermal populations of the higher spin states become significant at finite temperatures. This situation is the temperature-dependent paramagnetic state described by the Heisenberg model.[39,40] From our previous theoretical study,[29] this tendency was remarkable for chromium clusters **3** and **4**. However, the present UHF and DFT calculations clearly showed that the Mo(II)–Mo(II) bond is strong unless the intermetallic distance (R) exceeds 2.5 Å. Therefore, binuclear molybdenum complexes should be diamagnetic if $R<2.5$ Å,[13] while they should exhibit the temperature-dependent paramagnetism[7—12] in the region of $R>2.5$ Å, as shown in the preceding sections of MO-description and occupation numbers. In order to confirm this tendency, the effective direct exchange integrals (J_{ab}) for **1** were calculated by using an approximate spin-projection (AP)[30d] procedure for the UHF and DFT solutions in combination with the Heisenberg model:

$$J_{ab}(\text{APUHForAP-DFT}) = [E(\text{LS})-E(\text{HS})]/[\langle S^2\rangle(\text{HS})-\langle S^2\rangle(\text{LS})] \quad (5)$$

where the E(Y) and S^2(Y) denote, respectively, the total energy and total spin angular momentum for the spin state Y by UHF or DFT. It is noteworthy that the AP scheme is approximate but size-consistent.[29] On the other hand. the perfect-pairing (PP) type spin projection is inappropriate for calculations of J_{ab}[30,41] since it neglects the spin-decoupling (polarization) terms, which often play an essential role for subtle discussions of the HS–LS energy gaps[27] and the molecular magnetism.[42—44] Table 3 summarizes the J_{ab} values calculated for **1** by APUHF, APU-BLYP, APU-B2LYP, and APU-B3LYP. From Table 3, we draw the following conclusions:

(1) The effective exchange integrals calculated for **1** by all the methods are negative (antiferromagnetic), showing the covalent bond formation between the naked divalent molybdenum ion. The absolute values of those for **1** by all the methods are larger than 700 cm^{-1} if $R<2.5$ Å, showing the strong covalent bond formation between the divalent molybdenum ion.

(2) The magnitude of the J_{ab} values decreases with the increase of the Mo(II)–Mo(II) distance (R) in an exponential manner.

(3) The magnitude of the J_{ab} values shows the following tendency: $|J_{ab}(\text{APU-B2LYP})| > |J_{ab}(\text{APU-BLYP})| > |J_{ab}(\text{APUHF})|$.

(4) The J_{ab} values given by APU-B2LYP and APU-B3LYP are comparable with each other, indicating that the U-B2LYP method is sufficient for describing qualitatively the exchange interactions, though many parameters would be necessary for quantitative purposes.

From conclusion (1), one see that the d–d interaction between the Mo(II) ions is strong in conformity with the diamagnetism.[1—3] But, the elongation of the Mo(II)–Mo(II) bond beyond 2.5 Å induces the electron fluctuation and tem-

Table 3. The Effective Exchange Integrals (cm^{-1}) Calculated for the Mo(II) Dimer by the Approximate Spin Projected UHF, U-BLYP, U-B2LYP, and U-B3LYP Methods

R/Å	APUHF	APU-BLYP	APU-B2LYP	APU-B3LYP
2.000	−3225.	−3552.7	−4956.	−5031.
2.0981	−2444.	−3274.0	−3930.	−4018.
2.1208	−2291.	−3123.8	−3712.	−3808.
2.500	−737.8	−1281.3	−1421.3	−1489.1
3.000	−132.9	−346.5	−331.7	−380.7
3.500	−17.2	−121.0	−59.3	−97.7

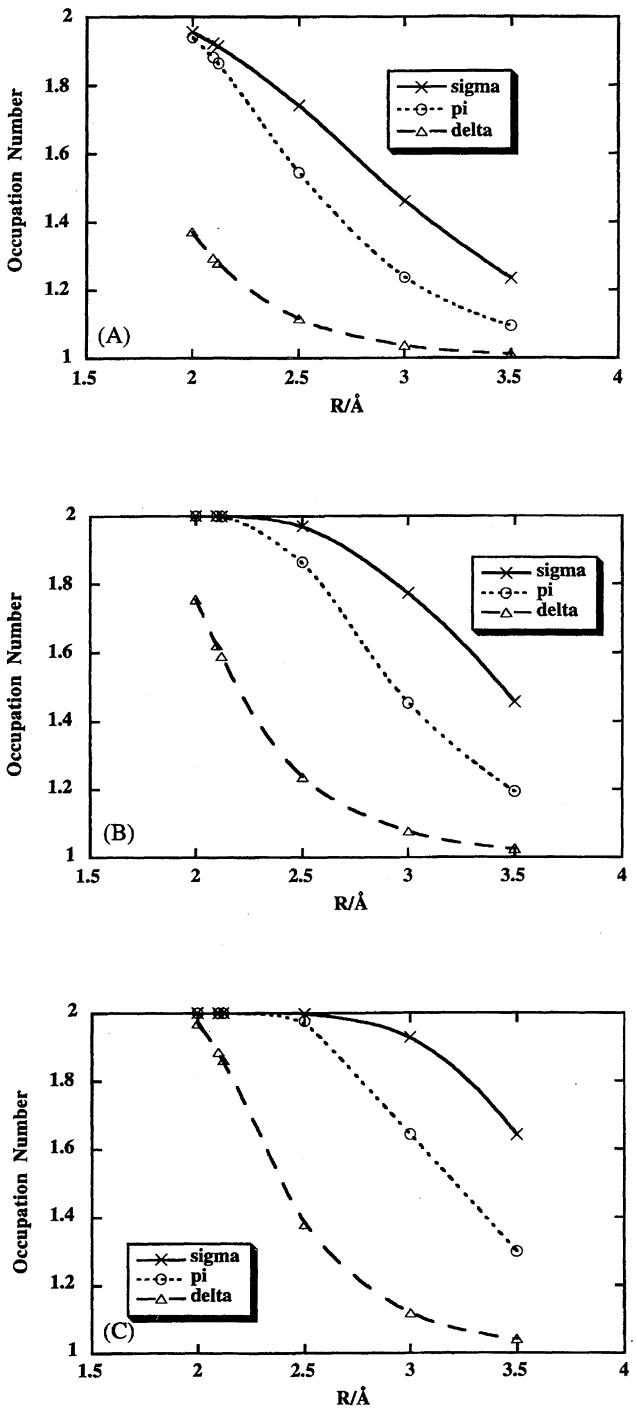

Fig. 4. Variations of the occupation numbers for the σ-, π-, and δ-type natural orbitals (UNO) with the interatomic distance (R). A, B, and C show the calculated values by the spin-projected (P) UHF, U-BLYP, and U-B2LYP methods.

perature-dependent paramagnetism. This is consistent with several experiments.[7—12]

CASCI Calculations by the Use of UNO

The spin-unrestricted approaches such as UHF and U-B2LYP often suffer the so-called spin-contamination errors.[27] The PP[25] and AP[30] spin projection procedures described above are utilized to remove them, particularly in the low spin (LS) state. However, the projection UHF and U-B2LYP are not applicable to the excited states in many cases. The configuration interaction (CI) or MCSCF calculations are necessary for well-balanced descriptions of the ground and lower-excited states, though they are impossible for larger clusters. Unfortunately, the GVB PP method, which is regarded as a simplified MCSCF, is not so effective for computations of the magnetic interactions.[30e] So, the complete active space (CAS) CI and CASSCF treatments involving the spin decoupling (polarization) terms are inevitable for the purpose.[46,47] UNOs are classified from the occupation numbers into three different groups; (1) core orbitals with n_i=2.0, (2) active orbitals where $0.0<n_i<2.0$, and (3) virtual orbitals with n_i=0.0. Therefore, the complete active space (CAS) among UNOs can be easily determined for a property under consideration. The full CI wave function Ψ within the UNO CAS is called UNO CASCI one,[27]

$$\Psi = \sum C_i \Phi_i \quad (i = 1\text{—full}), \tag{6}$$

where C_i and Φ_i denote UNO CASCI coefficient and configuration state function respectively. Judging from the occupation numbers, the eight active orbitals and eight electrons {8, 8} are at least necessary for the CASCI[46,47] calculations of **1** in order to confirm the APUHF and AP-DFT results. Here, UNOs determined by UHF were utilized for UNO CASCI calculation.[29] The UNO CASCI calculations were carried out using the HONDO 95 program package.[48]

In the above UHF and DFT calculations combined with the Heisenberg model,[27] all the σ-, π-, and δ-electrons were assumed to contribute to the temperature-dependent paramagnetism, giving an average J_{ab}-value over the five spin states. The CASCI calculations were performed to elucidate each energy difference between spin multiplets for **1** and also to elucidate the relative importance among σ-, π-, and δ-electrons for the paramagnetism. To this end, the J_{ab} values for the direct exchange coupling between the Mo(II) ions were calculated from total energies $E(Z)$ by UNO CASCI methods[27] as follows:

$$J_{ab}(1) = (E(S) - E(Q))/6 \tag{7a}$$

$$J_{ab}(2) = (E(T) - E(Q))/4 \tag{7b}$$

$$J_{ab}(3) = (E(S) - E(T))/2 \tag{7c}$$

where S, T, and Q (=Z) denote, respectively, the singlet, triplet, and quintet states. Therefore, if these J_{ab} values are nearly equal: $J_{ab} \cong J_{ab}(1) \cong J_{ab}(2) \cong J_{ab}(3)$, the energy splittings are reduced to those of the Heisenberg model, where all the σ-, π- and δ-electrons are assumed to be magnetic; $S_a=S_b=2$. Table 4 summarizes the $J_{ab}(1)$, $J_{ab}(2)$, and $J_{ab}(3)$ values obtained for **1** by UNO CAS CI {8,8} method.

From Table 4, one can draw the following conclusions:
(1) The calculated $J_{ab}(n)$ (n=1—3) values for **1** are largely negative in the region $R<2.5$ Å, showing that **1** is diamagnetic in nature.
(2) The absolute $J_{ab}(1)$, $J_{ab}(2)$, and $J_{ab}(3)$ values for **1** are quite different from each other in the region $R<2.5$ Å, showing the following tendency: $|J_{ab}(3)| < |J_{ab}(1)| < |J_{ab}(2)|$, in

Table 4. The Effective Exchange Integrals J_{ab} (cm^{-1}) Calculated for the Mo(II) Dimer by the Three Different Computational Procedures Based on the Total Energies by the UNO(UHF) CASCI Methods

R	UNO CASCI		
Å	$J_{ab}(1)$	$J_{ab}(2)$	$J_{ab}(3)$
2.0000	−5841.5	−7098.8	−3326.8
2.0981	−4425.1	−5375.5	−2524.3
2.1208	−4136.0	−5014.3	−2379.3
2.5000	−1097.5	−1156.2	−980.1
3.0000	−147.16	−147.33	−146.8
3.5000	−17.23	−17.24	−17.19

sharp contrast to those of **3**. Therefore, the energy splittings among the singlet (S), triplet (T), and quintet (Q) states are quite different from those obtained by the Heisenberg model assuming the localized spins: $S_a=S_b=2$.

(3) The magnitude of the $J_{ab}(3)$-value, which is mainly related to δ-orbitals, is only one-half of the $J_{ab}(2)$-value at R=2.0 Å. This means that only the δ-electron is rather weak in the Mo(II) dimer.

(4) The absolute $J_{ab}(1)$, $J_{ab}(2)$, $J_{ab}(3)$ values for **1** are almost equivalent in the region $R>2.5$ Å. The multiplet splittings become close to the Heisenberg type, showing the typical magnetic behavior.

(5) The $J_{ab}(1)$ by CASCI and J_{ab} by AP-UHF are close in the magnetic region ($R>2.5$ Å), showing the reliability of the approximate spin projection procedure.

(6) The magnitude of J_{ab} values by AP-UBLYP, -UB2LYP, and -UB3LYP becomes larger by several times than those of the CASCI and AP-UHF in the region ($R>3.0$ Å).

From these conclusions, we see that the Heisenberg model assuming that $S_a=S_b=2$ is not appropriate for **1** because of $|J_{ab}(3)|\neq|J_{ab}(1)|$. Thus, the nature of metal–metal bonds is quite different between Cr(II) and Mo(II) ions. A similar tendency is recognized for magnetic behaviors between first- and second-row transition metal ions in general.

The J_{ab} values in Tables 3 and 4 decrease with the increase of the Mo–Mo distance (R), as shown in Fig. 5. They can be fitted with the single exponential function with R

$$J_{ab} = -p \exp(-qR) \tag{8}$$

where p and q are the fitting parameters. The p and q values are -3.0×10^5 and 3.003 for $J_{ab}(3)$ by CASSCF, and -4.0×10^5 and 4.000 by UB2LYP, respectively. The absolute J_{ab} values estimated by both the methods become over 3000 cm^{-1} for **1** with short Mo–Mo bonds ($R<2.0$ Å), which are diamagnetic, in conformity with experiments.[1–3]

On the other hand, $|J_{ab}|$ values become smaller than 500 cm^{-1} if $R>2.5$ Å, and therefore the temperature-dependent paramagnetism should be important.[7–12] It is noteworthy that the DET method overestimates the magnitude of antiferromagnetic J_{ab} values in the magnetic region ($R>2.5$ Å).

Tetranuclear Mo(II) and Cluster Systems

1. Natural Orbitals, Occupation Numbers, and Bond Orders:

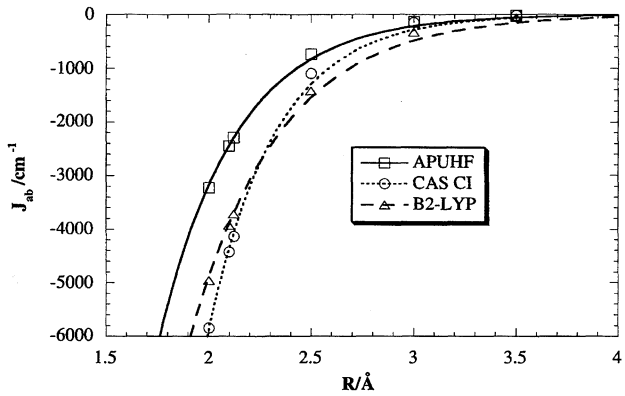

Fig. 5. Variations of calculated effective exchange integrals with interatomic distance (R) by APUHF and UNO CASCI {8,8}.

Mo(II)$_2$ dimer (**1**) has too strong d–d bonds for large electronic polarizations by the external electromagnetic fields. Exotic electronic properties arising from electron fluctuation may appear by elongation of d–d conjugated systems, as in the case of π–π conjugation in polyacetylene. Here, the linear equilateral tetramer {Mo(II)$_a$–Mo(II)$_b$–Mo(II)$_c$–Mo(II)$_d$} (**2**) of the Mo(II) ion with the equivalent interatomic distance was investigated to examine the d–d bond fluctuation using the SZ basis set.[31]

In principle, these d–d conjugated σ-, π-, and δ-type orbitals can be obtained by the extended Hückel[28] and spin-restricted DFT calculations.[22] Here, they were determined by the UHF and UB2LYP methods to incorporate static electron correlation effects.[29] Figure 6 shows the conjugated σ-, π-, and δ-type natural orbitals obtained by the UB2LYP method. The first-order density matrices obtained by these methods were diagonalized to obtain the natural orbitals and their occupation numbers for **2**.

Judging from the occupation numbers, we think that four valence orbitals should be active for each symmetry. Therefore sixteen active orbitals and sixteen active electrons are regarded as CAS {16,16} for **2** as well as for chromium tetramer (**4**). Since the UNO CASCI and CASSCF {16,16} calculations would be impossible at the present time, the spin-projected UHF and DFT calculations were carried out for a qualitative purpose. The four bonding DODS MOs for each symmetry are given by the mixing of the UNOs

$$\Psi_1^+(X) = \cos\theta_1\phi_1(X) + \sin\theta_1\phi_4(X) \tag{9a}$$

$$\Psi_2^+(X) = \cos\theta_2\phi_2(X) + \sin\theta_2\phi_3(X) \tag{9b}$$

where θ_i is the orbital mixing parameter for UNOs: $\phi_i(X)$: i=2(3) for HOMO(LUMO) and i=1(4) for the next HOMO(LUMO) with each symmetry. The UNOs are given by

$$\phi_i(X) = N[c_a dX_a + c_b dX_b + c_c dX_c + c_d dX_d] \quad (i = 1—4) \tag{10}$$

where c_f is the LCAO coefficient at the site f (=a,b,c,d) and N (N') is the normalizing factor. The occupation numbers for two π-bonding natural orbitals in Eq. 10 are calculated as described previously.[29]

Figure 7 illustrates variations of the occupation numbers

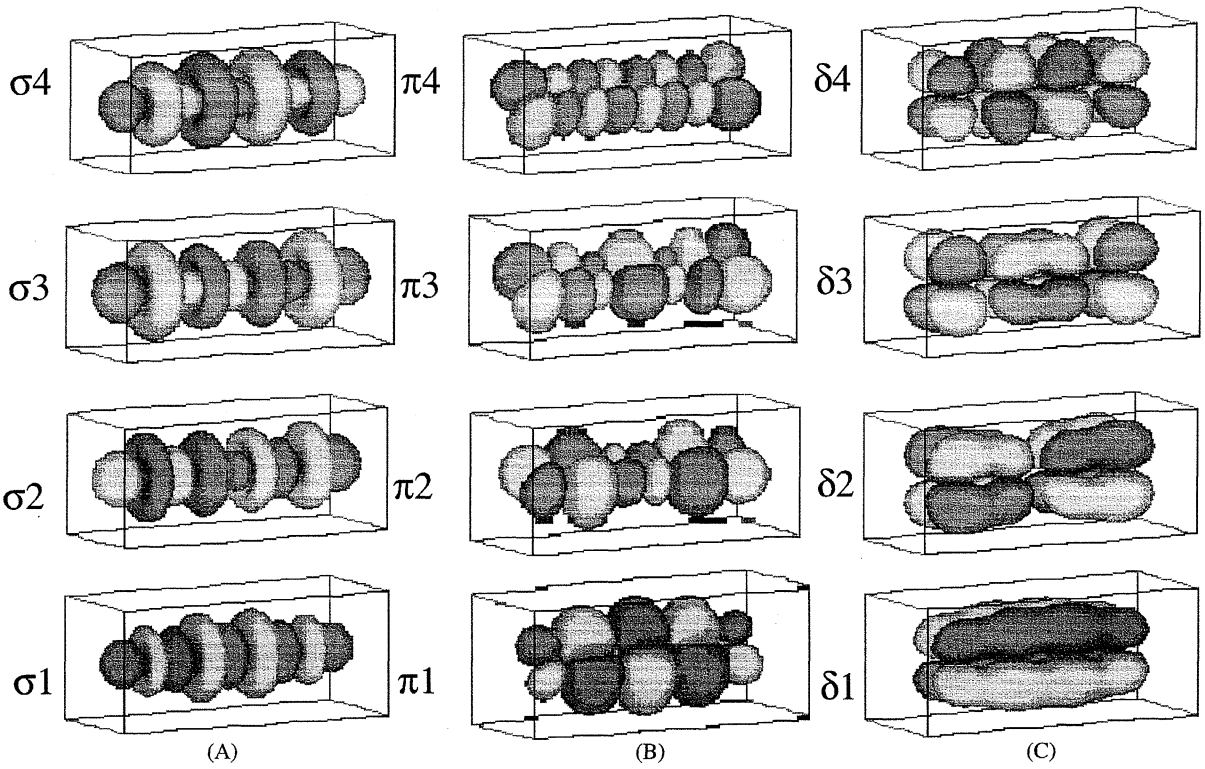

Fig. 6. The computer graphics of UNO for **2**. A, B, and C denote, respectively, σ, π, and δ-UNOs (see also Figs. 8 and 9).

with the change of the interatomic distance (R) for **2**. From Fig. 7, the following results are availabel:

(1) The occupation numbers for the HOMO with each symmetry by UHF are uniformly smaller than those of UB2LYP as are usuall in other cases.[29]

(2) The occupation numbers for the σ- and π-HOMOs are almost 2.0 in the region $R<2.2$ Å. This is ascribed to the strong d–d conjugation effect for Mo(II) ions.

(3) The occupation numbers for the σ-HOMO and the next σ-HOMO for **2** are larger than 1.5 even at R=2.5 Å under the UB2LYP approximation. The d–d conjugation effect is strong for the σ-orbitals. In fact, the σ-DODS MOs by UB2LYP are almost paired even at R=2.4 Å.

(4) The occupation number for the π-HOMO of **2** is smaller than the corresponding value for the σ-HOMO. The π-DODS MOs are therefore spin-polarized and are more or less localized on the left and right Mo(II) dimer groups of **2** at R=2.5 Å.

Conclusions (1) and (2) for the tetramer **2** are consistent with the metallic character. The sharp variations of the π-bond orders in the region; $2.3<R<2.7$ Å suggest that several electronic properties such as the hyperpolarizability and hypermagnetiability are controlable by changing the interatomic distances for the tetranuclear Mo(II) complexes with ligands and other structural factors.[37] Therefore experimental studies on electronic properties of the d–d conjugated systems are very interesting from this point of veiw.

2. Metal Insulator Transitions: In principle, the metal-metal distances are controlabel by chemical and physical techniques which arrange them. Here, let us elucidate how the DODS MOs given for **2** by Eq. 9 vary with the Mo(II)–Mo(II) distance (R). Figures 8, 9, and 10 illustrate their variations with R. These figures show that the delocalized closed-shell MO configuration (**10**) changes into the localized nonclosed-shell structure (**11**) (Scheme 3). For example, the σ-HOMOs for up- and down-spins are equivalent, closed-shell in nature, at R=2.0 Å, but they are slightly spin-polarized at R=2.5 Å, and finally they are almost localized on the left and right terminal Mo(II) atoms, respectively as shown in Fig. 8. This orbital bifurcation is much more remarkable in the case of π-bond. π-HOMOs for up- and down-spins are strongly paired, namely closed-shell in nature at R=2.0 Å, but they are quite spin-polarized even at R=2.5 Å, and they are almost localized on the left and right terminal Mo(II) atoms, respectively, as shown in Fig. 9. From Fig. 10, π-next HOMOs for up- and down-spins are also closed-shell at R=2.0 Å, but they are moderately spin-polarized at R=2.5 Å, and finally they are localized on the right and left inner Mo(II) atoms, respectively. Therefore, the π-electrons are localized so as to satisfy the antiferromagnetic spin alignment near the

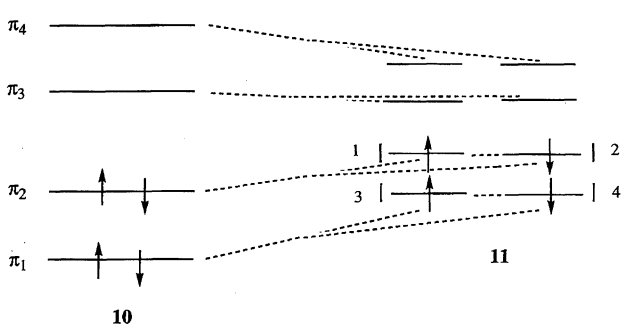

Scheme 3.

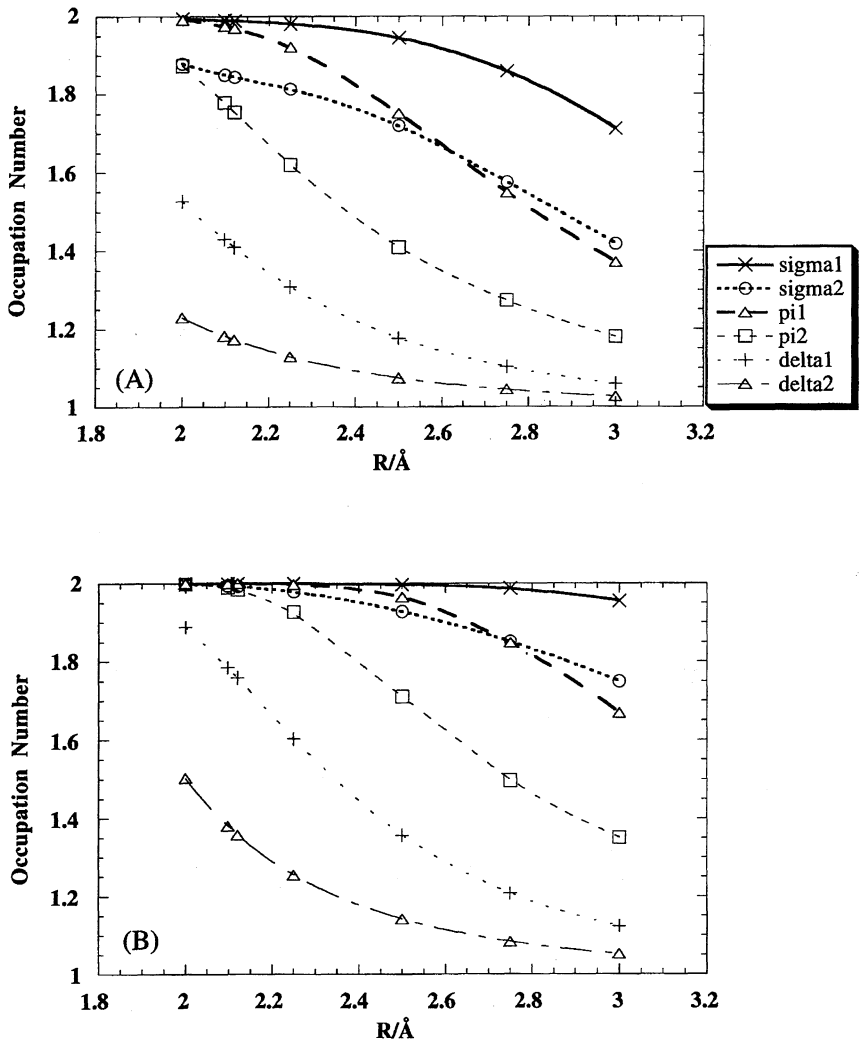

Fig. 7. Variations of the occupation numbers for the σ-, π-, and δ-type natural orbitals (UNO) with the interatomic distance (R). A and B show the calculated values by the spin-projected (P) UHF and U-B2LYP methods.

dissociation limit (**12**) (Scheme 4).

The above examples show that the bifurcation from the closed-shell MO to nonclosed-shell MO occurs near R=2.5 Å in the case of Mo(II) tetramer, though the Cr(II) tetramer remains magnetic even at R=2.0 Å. Probably the on-set region of the metal–insulator transitions is very interesting from the view point of electron fluctuation responsible for nonlinear optical phenomena,[37,38] while the magnetism is expected in the near dissociation region (R>2.5 Å) in accord with the experiments.[7—12]

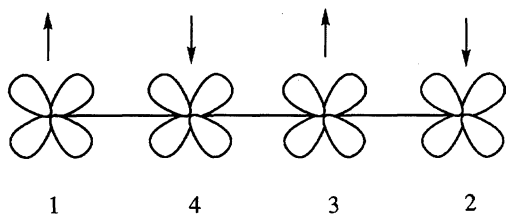

12

Scheme 4.

3. Spin Densities: The UHF and spin-polarized DFT calculations provide spin density alternation of the spin-density-wave (SDW)-type. But it disappears because of the very fast quantum spin tunneling (or fluctuation) in the case of small clusters such as **2**. In fact, the spin projection procedure is responsible for the isotropic rotation of the spin vector, retaining the antiferromagnetic spin correlation described by the scalar product of the spin vector **Sa**·**Sb**<0.[27] Tables 5A and 5B summarize, respectively, the total atomic spin densities (Q_f) obtained for **1** and **2** by UHF, U-BLYP, and U-B2LYP. From Table 5A, the magnitude of the calculated spin densities for **1** is quite different between UHF and U-B2LYP. The UHF calculation clearly overstimates the spin polarization on the inner Mo(II) atoms for **2**. On the other hand, the U-BLYP values would be too small because of the lack of the self-interaction correction (SIC).[32] It is well known that the DFT without SIC overstimates the stability of the antiferromagnetic state for copper oxides and other transition metal complexes. The magnitude of the atomic spin density on Mo(II) ions becomes almost 2.0 in the region:

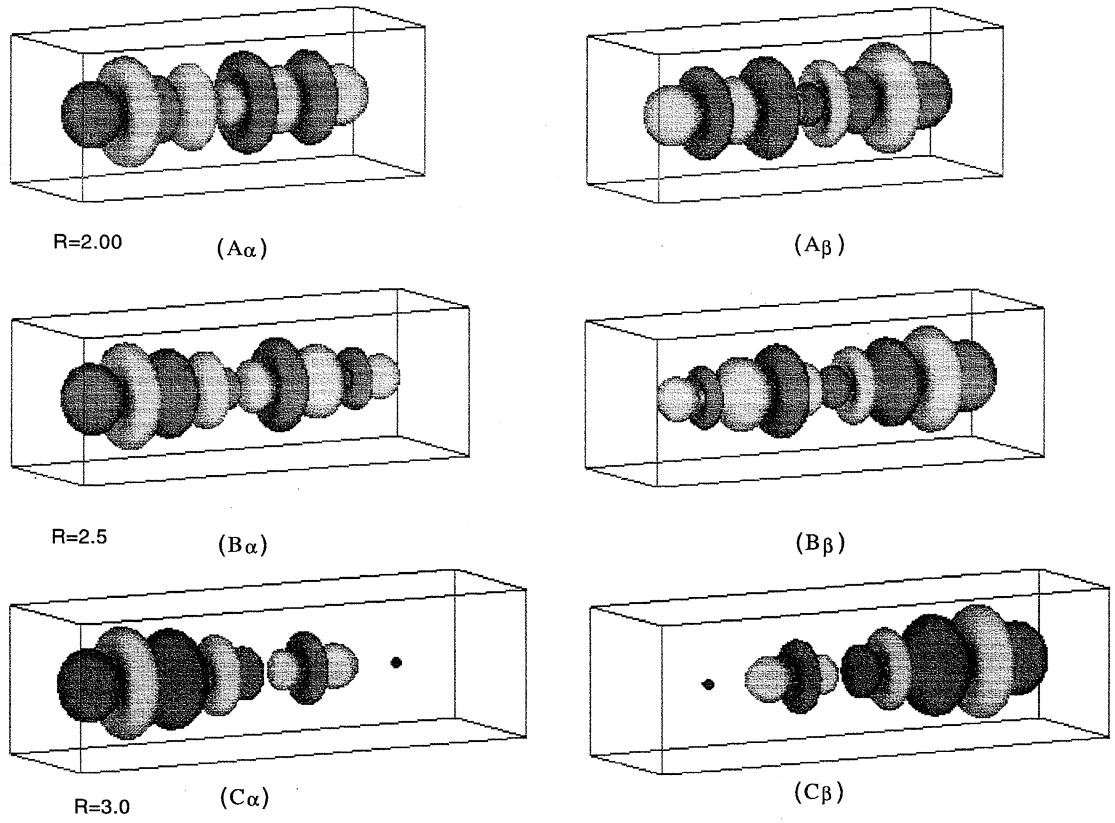

Fig. 8. The computer-graphics of σ-HOMOs for the Mo(II) tetramer (**2**) obtained the by the U-B2LYP method. A, B, and C denote, respectively, the σ-type HOMOs for the up (α) and down (β) spins at R=2.0, 2.5, and 3.0 Å.

Table 5. (A) Spin Densities for the Mo(II) Dimer (**1**)

R	UHF	UBLYP	U-B2LYP
Å	a(-b)	a(-b)	a(-b)
2.000	3.152	0.856	1.406
2.098	3.429	1.168	1.751
2.1208	3.479	1.231	1.850
2.500	3.918	2.555	3.325
3.000	4.030	3.648	3.871
3.500	4.025	3.934	3.982

(B) Spin Densities for the Mo(II) Tetramer (**2**)

R	UHF		B2LYP	
Å	a(-b)	b(-c)	a(-d)	b(-c)
2.000	3.107	−2.725	1.718	−1.389
2.096	3.327	−3.006	2.138	−1.732
2.098	3.331	−3.013	2.149	−1.740
2.1028	3.374	−3.074	2.249	−1.825
2.250	3.568	−3.372	2.741	−2.278
2.500	3.800	−3.751	3.316	−2.980
2.750	3.930	−3.951	3.606	−3.424
3.000	3.994	−4.035	3.755	−3.665

R<2.2 Å.

Discussions and Concluding Remarks

Bi- and Polynuclear Complexes: The quadruple bonds between Mo(II) ion are usually stable, exhibiting no magnetism.[1–3] The edge-sharing bioctahedral compounds of trivalent molybdenum with the d^3–d^3 interactions have usually stable $\sigma^2\pi^2\delta^2$ or $\sigma^2\pi^2(\delta^*)^2$ configurations with the diamagnetism. However, there are several unusual cases even for molybdenum complexes, as summarized in Table 6. The observed effective exchange integrals (J_{ab}) for several dimolybdenum compounds such as $Mo_2Cl_6(dppe)_2$[7–9] are in the range; −340——−470 cm^{-1}, exhibiting the temperature-dependent paramagnetism. Similarly, the face-sharing bioctahedral compounds of trivalent molybdenum, $[Mo(III)_2X_9]^{3-}$, showed that the Mo(III)–Mo(III) distances varied over the range 2.5—2.8 Å, depending on the crystalline environments.[10,12] These compounds exhibited a good correlation between the Mo–Mo distances and the paramagnetic susceptibilities,[7–12] in accord with that in Fig. 5. Thus the metal–insulator transitions induced by elongation of the Mo(II)–Mo(II) distance are explained by localizations of different-orbitals-for-different spins (DODS) MOs in Figs. 3, 4, 5, 8, 9, and 10 for **1** and **2**.[27]

Linear tetranuclear complexes with d–d conjugated bonds are in principle synthesized by chemical synthetic methods as has been performed by Mashima et al.[5,6] Both soft and hard ligands can be selectively used to arrange transition metal ions. Bi- and polynuclear complexes play important roles in bioinorganic chemistry.[49–52] The present computational methods will be applied to these systems elsewhere.

Low-Dimensional Systems: The present calculations

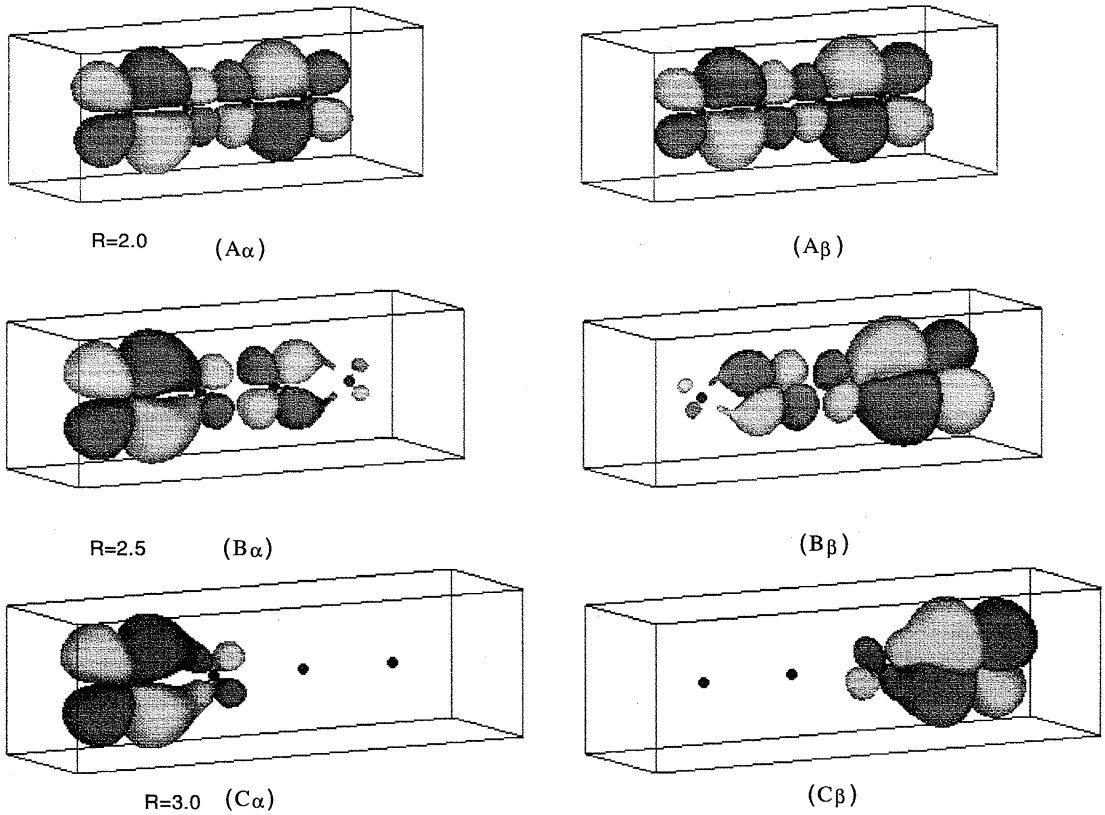

Fig. 9. The computer-graphics of the π-HOMOs for the Mo(II) tetramer (**2**) obtained the by the U-B2LYP method. A, B, and C denote, respectively, the π-type HOMOs for the up (α) and down (β) spins at R=2.0, 2.5, and 3.0 Å.

Table 6. The Observed J_{ab} (cm^{-1}) Values for Edge-Shared and Face-Shared Molybdenum Complexes

Edge-shared	d(Mo–Mo)	J_{ab}	Face-shared	d(Mo–Mo)	J_{ab}
$Mo_2Cl_4I_2(dppm)_2$	2.827	−875	$K_3Mo_2Cl_9$	2.524	−556
$Mo_2Br_6(dppm)_2$	2.879	−704	$Rb_3Mo_2Cl_9$	2.590	−491
$Mo_2I_7(dppm)_2$	3.061	−564	$Cs_3Mo_2Cl_9$	2.655	−414
$Mo_2Cl_6(dppm)_2$	2.789	−600	$(EtNH_3)_5MoCl_9$	2.670	−393
$Mo_2Cl_4(\mu SEt)_2(dpme)_2$	2.712	−340	$(PyH)_3Mo_2Cl_9$	2.685	−341
$Mo_2Cl_6(dppe)_2$	2.762	−471	$(PipeH)_3Mo_2Cl_9$	2.734	−267

show that the d–d bonds for binuclear Mo(II) complexes are too hard for electron fluctuations with the external fields. However, the HOMO-LUMO gaps become smaller from the d–d conjugation effect if the linear Mo(II) cluster sizes become larger. This implies that the d–d electron systems of larger low-dimensional Mo(II) cluster become soft (polarizable) when their sizes exceed a certain limit. The situation is similar in the case of polyenic systems.[29] Therefore the linear and ring clusters of Mo(II) ions and their analogs are particularly interesting from the view point of electronic, magnetic and optical properties as illustrated in Fig. 11. These systems could be formed by physical techniques developed recently. Probably the interatomic distances (R) are controlled, depending on properties under consideration, since their electronic structures change sharply with R. Mashima et al. have developed a new ligand (phphs) to synthesize the d–d conjugated systems such as M′–M=M–M′ (M=Cr(II), Mo(II); M′=Pd, Pt).[5,6] Probably another new ligand (L=A-B-C) would be necessary to synthesize the linear tetranuclear Mo(II) systems depicted in Fig. 11B. The Mo(II)–Mo(II) distances should be also controllable by choosing appropriate ligands. The oxidation and/or reduction of these d–d conjugated systems would be very interesting from the view point of cooperative phenomena of both charge and spin freedom. The present results show that the hybrid methods such as UB2LYP and UB3LYP method can be applicable for complex systems to elucidate such variations of electronic structures with R as illustrated in Figs. 8, 9, and 10.

The authors gratefully acknowledge the financial support of the Ministry of Education, Science, Sports and Culture (Specially Promoted Research No. 06101004).

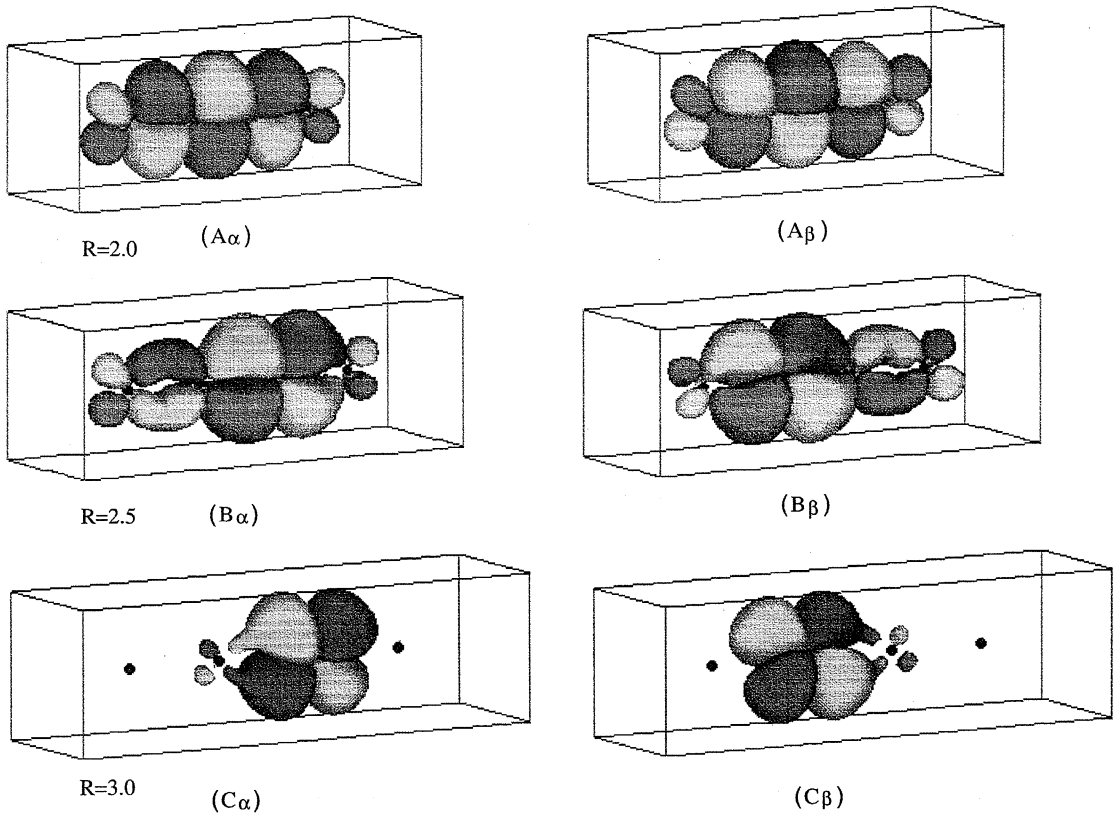

Fig. 10. The computer-graphics of the next π-HOMOs for the Mo(II) tetramer (**2**) obtained the by the U-B2LYP method. A, B, and C denote, respectively, the next π-type HOMOs for the up (α) and down (β) spins at R=2.0, 2.5, and 3.0 Å.

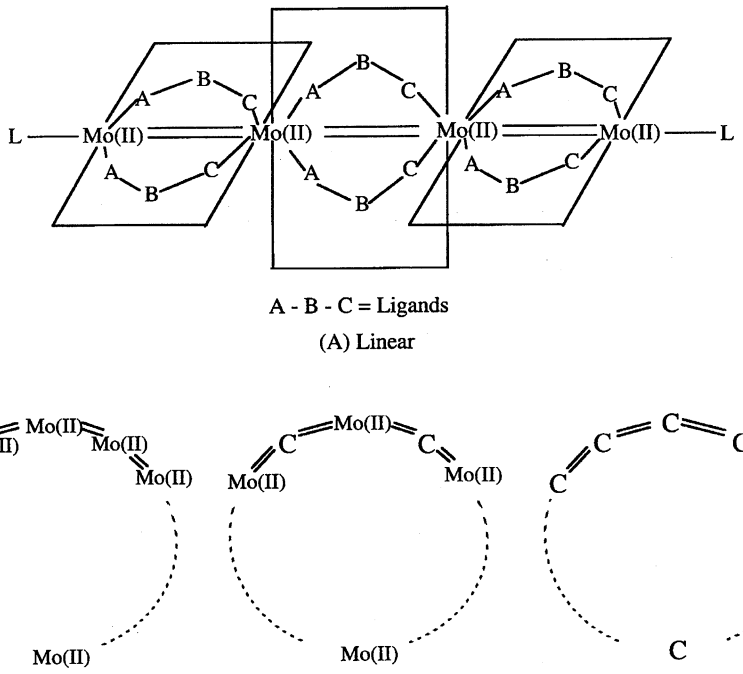

Fig. 11. Linear clusters (A) and ring clusters (B) of Mo(II) ions.

References

1) F. A. Cotton and R. A. Walton, "Multiple Bonds between Metal Atoms," Clarrendon Press, Oxford (1993), and references therein.

2) a) F. A. Cotton, *Acc. Chem. Res.*, **11**, 225 (1978); b) M. H. Chisholm and F. A. Cotton, *Acc. Chem. Res.*, **11**, 356 (1978).

3) a) F. A. Cotton and G. Wilkinson, "Advanced Inorganic Chemistry," 5th ed, John Wiley & Sons, New York; b) F. A. Cotton and R. A. Walton, "Multiple Bonds between Metal Atoms," Clarrendon Press, Oxford (1992), and references therein.

4) a) K. Sakai and K. Matsumoto, *J. Am. Chem. Soc.*, **111**, 3074 (1989); b) T. Taito, *Kagaku*, **43**, 274 (1989) (in Japanese).

5) a) K. Mashima, H. Nakano, and A. Nakamura, *J. Am. Chem. Soc.*, **115**, 11632 (1993); b) K. Mashima, H. Nakano, and A. Nakamura, *J. Am. Chem. Soc.*, **118**, 9083 (1996).

6) K. Mashima, M. Tanaka, K. Tani, A. Nakamura, S. Takeda, S. Mori, and K. Yamaguchi, *J. Am. Chem. Soc.*, **119**, 4307 (1997).

7) R. Poli and H. D. Mui, *Inorg. Chem.*, **28**, 3609 (1989).

8) P. A. Agaskar, F. A. Cotton, K. R. Dunbar, L. R. Falvello, and C. J. O'Conner, *Inorg. Chem.*, **26**, 4051 (1987).

9) F. A. Cotton, L. H. Daniels, K. R. Dunbar, L. R. Falvello, C. J. O'Conner, and A. C. Price, *Inorg. Chem.*, **30**, 2509 (1991).

10) R. Stranger, P. W. Smith, and I. E. Grey, *Inorg. Chem.*, **28**, 1271 (1989).

11) R. Poli and M. D. Mui, *Inorg. Chem.*, **30**, 65 (1991).

12) F. A. Cotton and R. L. Luck, *Inorg. Chem.*, **28**, 182 (1989).

13) K. Yamaguchi, *Chem. Phys. Lett.*, **66**, 395 (1979); **68**, 477 (1979).

14) A. P. Ginsberg, *J. Am. Chem. Soc.*, **102**, 111 (1980).

15) M.-H. Whangbo, M. J. Foshee, and R. Hoffmann, *Inorg. Chem.*, **19**, 1723 (1980).

16) a) C. D. Garner, I. H. Hillier, M. F. Guest, J. C. Green, and A. W. Coleman, *Chem. Phys. Lett.*, **41**, 91 (1976); b) M. F. Guest, I. H. Hillier, and C. D. Garner, *Chem. Phys. Lett.*, **48**, 587 (1977); c) M. F. Guest, C. D. Garner, I. H. Hillier, and I. B. Walton, *J. Chem. Soc., Faraday Trans.*, **74**, 2092 (1978); d) C. D. Garner, I. H. Hillier, M. J. Knight, A. A. MacDowell, J. B. Walton, and M. F. Guest, *J. Chem. Soc., Faraday Trans.*, **76**, 885 (1980); e) P. M. Atha, I. H. Hillier, and M. F. Guest, *Mol. Phys.*, **46**, 437 (1982); f) I. H. Hillier, *Pure Appl. Chem.*, **51**, 2183 (1979).

17) a) M. Benard, *J. Am. Chem. Soc.*, **100**, 2354 (1978); b) M. J. Benard, *J. Chem. Phys.*, **71**, 2546 (1979); c) M. Benard, P. Coppens, M. L. DeLucia, and E. D. Stevens, *Inorg. Chem.*, **19**, 1924 (1980); d) R. Weist and M. Benard, *Chem. Phys. Lett.*, **98**, 102 (1983); e) R. Weist and M. Benard, *Chem. Phys. Lett.*, **122**, 447 (1985).

18) F. A. Cotton and G. G. Stanley, *Inorg. Chem.*, **16**, 2668 (1977).

19) Y. Yoshioka, D. Yamaki, G. Maruta, T. Tsunesada, K. Takada, T. Noro, and K. Yamaguchi, *Bull. Chem. Soc. Jpn.*, **69**, 3395 (1996).

20) R. A. Kok and M. B. Hall, *J. Am. Chem. Soc.*, **98**, 102 (1983); b) R. A. Kok and M. B. Hall, *Inorg. Chem.*, **24**, 1542 (1985); c) M. B. Hall, *Polyhedron*, **6**, 679 (1987); d) D. D. Davy and M. B. Hall, *J. Am. Chem. Soc.*, **111**, 1268 (1989).

21) a) T. Ziegler, *J. Am. Chem. Soc.*, **106**, 5901 (1984); b) T. Ziegler, *J. Am. Chem. Soc.*, **107**, 4453 (1985); c) T. Ziegler, V. Tshinke, and A. Becke, *Polyhedron*, **6**, 685 (1987).

22) J. C. Slater, *Adv. Quant. Chem.*, **6**, 1 (1972).

23) D. L. Lichtenberger and J. G. Kristofzski, *J. Am. Chem. Soc.*, **109**, 3458 (1987).

24) R. D. Harcourt, F. L. Skrezenek, and G. A. R. Maclagan, *J. Am. Chem. Soc.*, **108**, 5403 (1986).

25) a) M. M. Googgame and W. A. Goddard, III, *Phys. Rev. Lett.*, **48**, 135 (1982); b) M. M. Googgame and W. A. Goddard, III, *J. Phys. Chem.*, **85**, 215 (1981).

26) K. E. Edgecombe and A. D. Becke, *Chem. Phys. Lett.*, **244**, 427 (1995).

27) K. Yamaguchi, in "Self-Consistent Field: Theory and Applications," ed by R. Carbo and M. Klobukowski, Elsevier, Amsterdam (1990), p. 727.

28) R. Hoffman, "Solids and Surface: A Chemist's View on Bonding in Extended Structures," VCH Pub., New York (1988).

29) a) M. Nishino, M. Tanaka, S. Takeda, K. Mashima, W. Wori, K. Tani, A. Nakamura, and K. Yamaguchi, *Mol. Cryst. Liq. Cryst.*, **286**, 193 (1996); b) M. Nishino, M. Tanaka, S. Takeda, K. Mashima, W. Wori, K. Tani, A. Nakamura, and K. Yamaguchi, *Mol. Cryst. Liq. Cryst.*, **286**, 200 (1996); c) M. Nishino, S. Yamanaka, Y. Yoshioka, and K. Yamaguchi, *J. Phys. Chem.*, **101**, 705 (1997).

30) a) K. Yamaguchi, T. Tsunekawa, Y. Toyoda, and T. Fueno, *Chem. Phys. Lett.*, **143**, 371 (1988); b) Y. Takahara, K. Yamaguchi, and T. Fueno, *Chem. Phys. Lett.*, **158**, 95 (1989); c) K. Yamaguchi, T. Fueno, K. Ueyama, A. Nakamura, and M.-A. Ozaki, *Chem. Phys. Lett.*, **168**, 56 (1990); d) K. Yamaguchi, Y. Takahara, and T. Fueno, in "Applied Quant. Chem.," ed by V. H. Smith, Jr., H. F. Schaefer, III, and K. Morokuma, Reidel, Dordrecht (1986), p. 155; e) S. Yamanaka, T. Kawakami, T. Noro, and K. Yamaguchi, *J. Mol. Struct. (Theochem)*, **310**, 185 (1994).

31) H. Tatewaki and S. Hujinaga, *J. Chem. Phys.*, **72**, 4339 (1980).

32) a) A. D. Becke, *Phys. Rev. A*, **38**, 3098 (1988); b) A. D. Becke, *J. Chem. Phys.*, **98**, 1372 (1993); c) K. E. Edgecombe and A. D. Becke, *Chem. Phys. Lett.*, **244**, 427 (1995).

33) C. Lee, W. Yamg, and R. G. Parr, *Phys. Rev. B*, **37**, 785 (1988).

34) M. J. Frisch, G. W. Trucks, H. B. Schlegel, P. M. W. Gill, B. G. Johnson, M. A. Robb, J. R. Cheeseman, T. A. Keith, G. A. Petersson, J. A. Montgomery, K. Raghavachari, M. A. Al-Laham, V. G. Zakrewski, J. V. Ortiz, J. B. Foresman, J. Cioslowski, B. B. Stefanov, A. Nanayakkara, M. Challacombe, C. Y. Peng, P. Y. Ayala, W. Chen, M. W. Wong, J. L. Andres, E. S. Replogle, R. Gomperts, R. L. Martin, D. J. Fox, J. S. Binkley, D. J. Defrees, J. Baker, J. P. Stewart, M. Head-Gordon, C. Gonzalez, and J. A. Pople, Gaussian Inc., Pittsburgh, PA (1995).

35) K. Yamaguchi, *Chem. Phys. Lett.*, **33**, 330 (1975).

36) K. Takatsuka, T. Fueno, and K. Yamaguchi, *Theoret. Chim. Acta*, **48**, 187 (1978).

37) a) N. J. Long, *Angew. Chem., Int. Ed. Engl.*, **34**, 21 (1995); b) Y. Wada and M. Yamashita, *Jpn. J. Appl. Phys.*, **29**, 2744 (1990); c) I. R. Whittall et al., *Organometallics*, **14**, 3970, 5493 (1995); d) K. Mashima et al., *Chem. Lett.*, **1997**, 411 (1997).

38) M. Nakano, I. Shigemoto, S. Yamada, and K. Yamaguchi, *J. Chem. Phys.*, **103**, 4175 (1995).

39) G. C. Campbell and J. F. Haw, *Inorg. Chem.*, **27**, 3706 (1988).

40) a) F. A. Cotton, J. L. Eglin, B. Hong, and C. A. James, *J. Am. Chem. Soc.*, **114**, 4915 (1992); b) F. A. Cotton, L. Chen, L. M. Daniels, and X. Feng, *J. Am. Chem. Soc.*, **114**, 8980 (1992).

41) S. Yamanaka, T. Kawamura, T. Noro, and K. Yamaguchi, *J. Mol. Struct. (Theochem)*, **310** 185 (1994).

42) R. D. Willett, D. Gattechi, and O. Kahn, "Magneto-Structural Correlations in Exchange Coupled Systems," Reidel, Boston, MA (1985).

43) J. S. Miller and A. J. Epstein, *Mol. Cryst. Liq. Cryst.*, **271**, 272 (1995).
44) D. Gatteschi, O. Kahn, J. S. Miller, and F. Palacio, "Magnetic Molecular Materials," NATO ASDI Series, Kluwer Academic Publishers, Hague (1991), Vol. 198.
45) E. Coronado, "Molecular Magnetism: From Molecular Assembkies to the Devices," NATO ASI Series, Kluwer Academic Publishers, Hague (1996).
46) K. Yamaguchi, *Int. J. Quant. Chem.*, **S14**, 267 (1980).
47) a) P. Pulay and T. P. Hamilton, *J. Chem. Phys.*, **88**, 4926 (1988); b) J. M. Bofill and P. Pulay, *J. Chem. Phys.*, **90**, 3657 (1989).
48) M. Dupuis, A. Marquez, and E. R. Davidson, "HONDO 95.3 from CHEM-Station," IBM Corporation, Neighborhood Road, Kingston, NY (1995), p. 12401.
49) R. E. Carlin, "Magnetochemistry," Springer-Verlag, New York (1986).
50) S. J. Lippard, *Angew. Chem., Int. Ed. Engl.*, **27**, 344 (1988).
51) L. Que, "Metal Clusters in Proteins," ACS Symposium Series 372, ACS, Washington, DC (1988).
52) E. I. Stiefel and K. Matsumoto, "Transition Metal Sulfur Chemistry," ACS Symposium Series 653, ACS, Washington, DC (1996).